

Interpolatory Methods for Generic BizJet Gust Load Alleviation Function

C. Poussot-Vassal, P. Vuillemin, O. Cantinaud and F. Sève ^{*†}

December 21, 2020

Abstract

The paper's main contribution concerns the use of interpolatory methods to solve end to end industrial control problems involving complex linear dynamical systems. More in details, contributions show how the rational data and function interpolation framework is a pivotal tool *(i)* to construct (frequency-limited) reduced order dynamical models appropriate for model-based control design and *(ii)* to accurately discretise controllers in view of on-board computer-limited implementation. These contributions are illustrated along the paper through the design of an active feedback gust load alleviation function, applied on an industrial generic business jet aircraft use-case. The closed-loop validation and performances evaluation are assessed through the use of an industrial dedicated simulator and considering certification objectives. Although application is centred on aircraft applications, the method is not restrictive and can be extended to any linear dynamical systems.

1 Introduction

1.1 General aircraft context

Aircraft mobility plays an important role in our life style and societal organisation. As this transportation mean is facing severe environmental and societal challenges (*e.g.* global warming and CO₂ emissions), it is the role of researchers to provide innovative answers and industry-oriented tools to address them. These solutions should fulfil the safety and design requirements and be numerically efficient and simple to implement within the aircraft industrial design value chain. Among others scientific disciplines, it is well admitted that civil aircraft industry relies on dynamical systems theory, linear algebra and computational sciences to address these issues. In light of these statements, recent developments in these scientific communities may have a major impact in the overall aircraft conception and exploitation enhancement [2, 45]. Hopefully, it can also be a substantial lever in the *civil aviation footprint reduction*. This is one of the main expectation of this work.

In order to reach these ambitious objectives, the paper highlights the pivotal role and relevance of *interpolatory methods* [4, 5] in the context of *linear time invariant (LTI) large-scale systems* [34].

1.2 Generic business jet aircraft context

More specifically, through a complete industrial gust load alleviation control design and validation problem applied to a generic business jet aircraft, we show how rational function interpolation is

^{*}C. Poussot-Vassal and P. Vuillemin are with Université de Toulouse, F-31055 Toulouse, France. Contact: charles.poussot-vassal@onera.fr. O. Cantinaud and F. Sève are with Dassault-Aviation, France.

[†]This work has been funded within the frame of the Joint Technology Initiative JTI Clean Sky 2, AIRFRAME Integrated Technology Demonstrator platform AIRFRAME ITD (contract N. CSJU-CS2-GAM-AIR-2014-15-01 Annex 1, Issue B04, October 2nd, 2015) being part of the Horizon 2020 research and Innovation framework program of the European Commission.

an appealing ingredient for engineers. It is used *(i)* to construct *reduced order dynamical models* appropriate for feedback control design and *(ii)* to compute more accurate *sampled-time* gust load dynamical controller functions that can be implemented in a constrained on-board computer. The complete closed-loop stability and performance analysis is done through a dedicated *industrial simulator* to assess the approach.

1.3 Generic business gust load alleviation feedback control objective

An important aircraft design criteria concerns the *gust load envelope* that should not reach some limit to ensure structure integrity. To this aim, it is standard considering vertical gusts wavelengths, modelled through the following "1-cosine" profile

$$\mathbf{w}_g(t) = \begin{cases} \frac{W}{2} \left(1 - \cos \left(\frac{\pi V}{L} t \right) \right) & \text{for } 0 \leq t \leq \frac{2L}{V} \\ 0 & \text{for } t > \frac{2L}{V} \end{cases}, \quad (1)$$

where W is the gust velocity (in feet), L is the gust wavelength (in meters) and V is the aircraft true airspeed (in meter per seconds)¹. The *gust load envelope* is simply the worst case load responses along the wing span in reaction to the set of time-domain vertical wind gust profiles eq. (1) affecting the aircraft. Similarly to aerodynamical effects inducing vibrations [25], these gusts represent typical phenomena the aircraft might face during its exploitation. Prior any flight test, aircraft manufacturers should guarantee authorities that they can be handled by the system.

In the preliminary conception step (before considering any control functions), the aircraft is designed by experts so that the wings should support a given nominal load envelope, dictated by physical considerations such as desired aircraft manoeuvrability, gust, and many other manufacturing constraints. The larger the supported loads are, the larger the structural stiffeners and mass reinforcements should be. The aircraft mass is consequently bigger and its consumption during flight increased. In this context, the *Gust Load Alleviation* (GLA) control function plays an important role in the aircraft conception: it is aimed at lowering the loads envelope and thus at reducing the aircraft overall mass, consumption and emissions [1, 14]. In this work, the gain brought by the GLA, on the *worst upward gain* is denoted by $\mathcal{E}(x_i)$, is computed as

$$\mathcal{E}(x_i) = \max_{\mathbf{w}_g \in \mathcal{W}} \left\| \frac{\mathbf{z}_{\text{loads}}(x_i) - \mathbf{z}_{\text{loads}}^{(\text{GLA})}(x_i)}{\mathbf{z}_{\text{loads}}(x_i)} \right\|_{\infty}, \quad (2)$$

where x_i (in meters) is the wing location points where the loads are computed (here five locations $x_i = [x_1, x_2, x_3, x_4, x_5]\text{m}$) and where \mathcal{W} is the set of gust profiles as in (1). Then, $\mathbf{z}_{\text{loads}}(x_i)$ denotes the load at location x_i for the baseline aircraft and $\mathbf{z}_{\text{loads}}^{(\text{GLA})}(x_i)$ denotes the one when the *Gust Load Alleviation* (GLA) control function is activated. Both responses are obtained when the aircraft model is fed by eq. (1) (see also section 2).

1.4 Generic business gust load alleviation feedback industrial constraints

In an industrial value chain, the GLA function is traditionally designed after the flight controller (focusing on handling qualities). Then, one requirement is that GLA control should not impact the nominal (low frequencies) flight performances and focus on the gust phenomena and load envelope only. In addition, as the control functions should be implemented in a limited sampled-time computer, with a constrained material architecture (sensors and actuators limitations, sampling limitations, delays in the loop, *etc.*), the discretisation step should also be accurately taken into account before any implementation and performance evaluation.

¹Typical values for these parameters are provided by authorities and results in hundreds of different gust configurations.

1.5 Main results and paper organisation

Given the above considerations and objectives, the rest of the paper is focused on the central role of the *interpolation* applied to the *gust load alleviation control* problem. The paper is organised as follows. The gust load-oriented aircraft modelling is detailed in section 2, leading to a set of medium-scale irrational models. As the main mathematical tool involved here, reminders on the interpolation framework are recalled in section 3. Its application for the construction of rational reduced order models set, suitable for linear control design, is described in section 4. Then, after briefly describing the continuous-time GLA controller synthesis and the continuous and sampled-time interconnection framework, the controller *discretisation* through the interpolation framework is detailed in section 5. This last point stands as a methodological contribution of the work. Finally, conclusions are given in section 6, illustrating first the efficiency of the proposed process to alleviate gust-driven loads in an industrial application context, and second, to summarise the main contributions that can be applied to any kind of linear dynamical models.

Although the paper is centred around the aircraft gust load function, the proposed approach is readily applicable to any other aircraft control problems (including aircraft flight quality, vibrations, *etc.* functions). It is also valid to (m)any linear time invariant dynamical use-cases. Indeed, the presented *interpolatory framework* versatility allows to address a large number of engineering applications.

1.6 Notations

Let us denote by \mathbb{R} the set of real numbers, \mathbb{C} the set of complex numbers, \mathbb{C}_+ (\mathbb{C}_-) the open right (left) half plane, \mathcal{D} the open unit disk, $\partial\mathcal{D}$ its boundary and $\overline{\mathcal{D}}$ the complementary of the closed unit disk, respectively. The complex variable is given by $\iota = \sqrt{-1}$. Let $\mathcal{L}_2(\mathcal{I})$ ($\mathcal{I} = \iota\mathbb{R}$ or $\partial\mathcal{D}$) be the set of functions that are square integrable on \mathcal{I} . Let $\mathcal{H}_2(\mathcal{D})$ (resp. $\mathcal{H}_2(\overline{\mathcal{D}})$) be the subset of $\mathcal{L}_2(\partial\mathcal{D})$ containing the functions analytic in \mathcal{D} (resp. $\overline{\mathcal{D}}$). Let $\mathcal{H}_2(\mathbb{C}_+)$, shortly \mathcal{H}_2 , (resp. $\mathcal{H}_2(\mathbb{C}_-)$) be the subset of $\mathcal{L}_2(\iota\mathbb{R})$ containing the functions analytic in \mathbb{C}_+ (resp. \mathbb{C}_-). Similarly, let $\mathcal{L}_\infty(\mathcal{I})$ ($\mathcal{I} = \iota\mathbb{R}$ or $\partial\mathcal{D}$) be the set of functions that are bounded on \mathcal{I} . Let $\mathcal{H}_\infty(\mathcal{D})$ (resp. $\mathcal{H}_\infty(\overline{\mathcal{D}})$) be the subset of $\mathcal{L}_\infty(\partial\mathcal{D})$ containing the functions analytic in \mathcal{D} (resp. $\overline{\mathcal{D}}$) and $\mathcal{H}_\infty(\mathbb{C}_+)$, shortly \mathcal{H}_∞ , the subset of $\mathcal{L}_\infty(\iota\mathbb{R})$ of functions analytic in \mathbb{C}_+ . The Fourier transform of a time-domain signal $v \in \mathcal{L}_2(\mathbb{R})$ is denoted by $\bar{v} = \mathcal{F}(v)$.

2 Gust load oriented modelling

fig. 1 illustrates the considered feedback control loop architecture, where the sampled-time GLA function denoted as "GLA controller" is to be computed and validated. One may note that the actuators, sensors, flight controller and computational delay are considered as given and included in the considered generic business jet (BizJet) aircraft model set, referred to as $\{\mathbf{G}_i\}_{i=1}^{n_s}$, and detailed hereafter.

In section 2.1, the large-scale aeroservoelastic models $\{\mathbf{G}_i\}_{i=1}^{n_s}$, as provided by physics and loads teams, is described. Its input-output simplification is then done in section 2.2, leading to the the set of irrational models $\{\mathbf{H}_i\}_{i=1}^{n_s}$.

2.1 Aeroservoelastic aircraft modelling

To guarantee the safety and performance levels, GLA function is developed using very accurate environment and models, issued from aeroservoelastic modelling teams [31, 33, 32, 20].

Following fig. 1, $\{\mathbf{G}_i\}_{i=1}^{n_s}$ denotes the gust load oriented dynamical models family complex-valued functions. Each \mathbf{G}_i ($i = 1, \dots, n_s$) represents a *linear time invariant dynamical model* of the aircraft, evaluated at a given flight and mass condition. Its construction is a know-how of the aircraft manufacturer and usually results from multiple steps performed by different experts from fluid mechanics, structural, tests *etc.* teams. Each model $\{\mathbf{G}_i\}_{i=1}^{n_s}$ is described by the following

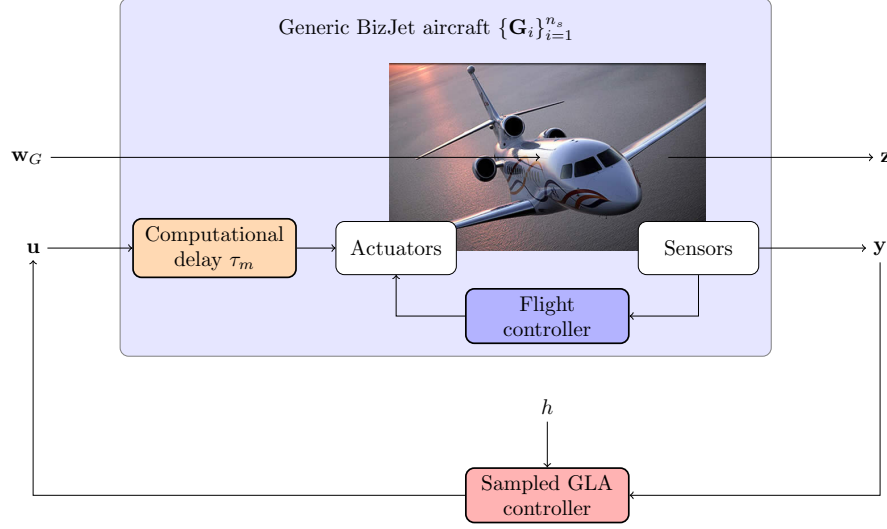


Figure 1: Closed-loop architecture of the GLA problem. The complete aeroservoelastic dynamical aircraft models $\{\mathbf{G}_i\}_{i=1}^{n_s}$ include the "Flight controller", "Actuators", "Sensors" and "Computational delay τ_m ". The "GLA controller" is GLA function to be computed. Signals \mathbf{w} , \mathbf{u} , \mathbf{z} and \mathbf{y} denote the exogenous inputs, control inputs, performance outputs and measurements, respectively. Then h denotes the sampling time used in the GLA function.

realisation denoted by $\{\mathcal{G}_i\}_{i=1}^{n_s}$

$$\{\mathcal{G}_i\}_{i=1}^{n_s} : \begin{cases} \dot{\mathbf{x}}^{(i)}(t) &= A^{(i)}\mathbf{x}^{(i)}(t) + B^{(i)} \begin{bmatrix} \mathbf{w}_G(t) \\ \mathbf{u}(t) \end{bmatrix} \\ \begin{bmatrix} \mathbf{y}(t) \\ \mathbf{z}(t) \end{bmatrix} &= C^{(i)}\mathbf{x}^{(i)}(t) + C_d^{(i)}\mathbf{x}^{(i)}(t - \tau_m) \end{cases} \quad (3)$$

where $\mathbf{x}^{(i)}(t) \in \mathbb{R}^{M_i}$, $\mathbf{u}(t) \in \mathbb{R}^{n_u}$, $\mathbf{w}_G(t) \in \mathbb{R}^{n_{wG}}$, $\mathbf{y}(t) \in \mathbb{R}^{n_y}$ and $\mathbf{z}(t) \in \mathbb{R}^{n_z}$ are the internal variables, input, exogenous input, output and performance output signals, respectively. The dimensions n_u , n_{wG} , n_y and n_z are constant for all n_s models, while M_i depends on the model configuration ($i = 1, \dots, n_s$). Finally, $\tau_m \in \mathbb{R}_+$ represents the computational delay needed to capture the \mathbf{y} signal (and to compute the - to be designed - GLA control law).

In the considered use-case, \mathbf{u} gathers three control inputs, the horizontal tail, the inner and outer ailerons ($n_u = 3$). Exogenous input \mathbf{w}_G gathers δ_{mc}^* , the aircraft horizontal tail deflection given by the pilot, the gust disturbance and its first and second derivatives, applied at three different locations of the aircraft fuselage ($n_w = 7$). This vector reads

$$\mathbf{w}_G(t) = \begin{bmatrix} \delta_{mc}^*(t), \underbrace{\mathbf{w}_g(t), \dot{\mathbf{w}}_g(t), \ddot{\mathbf{w}}_g(t)}_{\text{aircraft front}}, \underbrace{\mathbf{w}_g(t - \tau_1^{(i)}), \dot{\mathbf{w}}_g(t - \tau_1^{(i)}), \ddot{\mathbf{w}}_g(t - \tau_1^{(i)})}_{\text{aircraft middle}}, \dots, \underbrace{\mathbf{w}_g(t - \tau_2^{(i)}), \dot{\mathbf{w}}_g(t - \tau_2^{(i)}), \ddot{\mathbf{w}}_g(t - \tau_2^{(i)})}_{\text{aircraft rear}} \end{bmatrix}^T, \quad (4)$$

where the same gust (position, velocity and acceleration) enters in the model at the front, the middle and the rear, with a delay $\tau_1^{(i)} \in \mathbb{R}_+$ and $\tau_2^{(i)} \in \mathbb{R}_+$, depending on the aircraft velocity ($i = 1, \dots, n_s$). The only considered measurement \mathbf{y} is the aircraft angle of attack at the nose level ($n_y = 1$). Finally, the performances \mathbf{z} gathers outputs being the tracking signal error between the load factor without (\mathbf{n}_z^*) and with (\mathbf{n}_z) GLA controller $\mathbf{n}_z^* - \mathbf{n}_z$ and the loads envelope $\mathbf{z}_{\text{loads}}(x_i)$ ($n_z = 6$). The $A^{(i)}$, $B^{(i)}$, $C^{(i)}$ and $C_d^{(i)}$ matrices are real and of appropriate dimensions.

2.2 Toward gust load control-oriented models

As signals in eq. (4) are repeated and linked together, it can be problematic to deal with in a control design setup. One solution is to merge them in order to deal with $\mathbf{w}(t) = [\delta_{mc}^*(t), \mathbf{w}_G(t)]^T$ instead of eq. (4). This can be obtained by applying the following simple transformation

$$\begin{bmatrix} \delta_{mc}^*(t) \\ \mathbf{w}_g(t) \\ \dot{\mathbf{w}}_g(t) \\ \ddot{\mathbf{w}}_g(t) \\ \mathbf{w}_g(t - \tau_1^{(i)}) \\ \dot{\mathbf{w}}_g(t - \tau_1^{(i)}) \\ \ddot{\mathbf{w}}_g(t - \tau_1^{(i)}) \\ \mathbf{w}_g(t - \tau_2^{(i)}) \\ \dot{\mathbf{w}}_g(t - \tau_2^{(i)}) \\ \ddot{\mathbf{w}}_g(t - \tau_2^{(i)}) \end{bmatrix} = \begin{bmatrix} 1 & 0 \\ 0 & 1 \\ 0 & s \\ 0 & s^2 \\ 0 & e^{-\tau_1^{(i)}s} \\ 0 & se^{-\tau_1^{(i)}s} \\ 0 & s^2e^{-\tau_1^{(i)}s} \\ 0 & e^{-\tau_2^{(i)}s} \\ 0 & se^{-\tau_2^{(i)}s} \\ 0 & s^2e^{-\tau_2^{(i)}s} \end{bmatrix} \begin{bmatrix} \delta_{mc}^*(t) \\ \mathbf{w}_G(t) \end{bmatrix}, \quad (5)$$

where s denotes the Laplace variable. By merging eq. (3) and eq. (5), one can now re-construct each model in a realisation form $\{\mathcal{S}_i\}_{i=1}^{n_s}$ as

$$\{\mathcal{S}_i\}_{i=1}^{n_s} : \begin{cases} E^{(i)}\dot{\mathbf{x}}^{(i)}(t) &= A_0^{(i)}\mathbf{x}^{(i)}(t) + A_1^{(i)}\mathbf{x}^{(i)}(t - \tau_1^{(i)}) + A_2^{(i)}\mathbf{x}^{(i)}(t - \tau_2^{(i)}) \\ &+ B_g^{(i)} \begin{bmatrix} \mathbf{w}(t) \\ \mathbf{u}(t) \end{bmatrix} \\ \begin{bmatrix} \mathbf{y}(t) \\ \mathbf{z}(t) \end{bmatrix} &= C_0^{(i)}\mathbf{x}^{(i)}(t) + C_1^{(i)}\mathbf{x}^{(i)}(t - \tau_m) \end{cases} \quad (6)$$

where $\mathbf{x}^{(i)}(t) \in \mathbb{R}^{N_i}$, $\mathbf{u}(t) \in \mathbb{R}^{n_u}$, $\mathbf{w}(t) \in \mathbb{R}^{n_w}$, $\mathbf{y}(t) \in \mathbb{R}^{n_y}$ and $\mathbf{z}(t) \in \mathbb{R}^{n_z}$ are the internal variables, input, exogenous input, output and performance output signals, respectively. With this new form n_u , n_y and n_z are unaffected, while $n_w = 2$ (instead of 10 in eq. (4)) and $N_i = M_i + 6$, due to the double derivative and delay structure added. The $E^{(i)}$, $A_0^{(i)}$, $A_1^{(i)}$, $A_2^{(i)}$, $B_g^{(i)}$, $C_0^{(i)}$ and $C_1^{(i)}$ matrices are real and of appropriate dimensions.

Remark 1 (About the internal delays $\tau_1^{(i)}$ and $\tau_2^{(i)}$, and the $E^{(i)}$ matrix rank) *In the considered use-case, the fuselage is subdivided in three patches. Consequently, the gust vertical displacement signal $\mathbf{w}_g(t)$ given in eq. (1), enters the model at t , $t + \tau_1^{(i)}$ and $t + \tau_2^{(i)}$ ($0 < \tau_1^{(i)} < \tau_2^{(i)}$). To consider one single gust input signal (instead of three delayed), internal delay are added in the model. Similarly, to be able to accurately compute the loads along the wings, the model must take as gust input, its vertical displacement as in eq. (1), and its first and second derivatives as in eq. (4) [33]. Once again, to limit the model number of input disturbances to one instead of three (position, velocity and acceleration), the first and second derivatives of eq. (1) are embedded in the model, leading to a descriptor form as in eq. (6). More specifically, in our case, the $E^{(i)}$ matrix rank is then equal to $N_i - 6$: two rank loss per fuselage patch (one for the first and one for the second derivative).*

Following $\{\mathcal{S}_i\}_{i=1}^{n_s}$ given in equation eq. (6), the gust load oriented model is a family of dynamical models which transfer function $\{\mathbf{H}_i\}_{i=1}^{n_s}$, from \mathbf{u} and \mathbf{w} to \mathbf{y} and \mathbf{z} , reads

$$\mathbf{H}_i(s) = \left(C_0^{(i)} + C_1^{(i)} e^{-\tau_m^{(i)}s} \right) \left(sE^{(i)} - A_0^{(i)} - A_1^{(i)} e^{\tau_1^{(i)}s} - A_2^{(i)} e^{\tau_2^{(i)}s} \right)^{-1} B^{(i)}. \quad (7)$$

3 Preliminaries in rational interpolation and approximation

The entire proposal relies on a specific use of the model interpolation tools: namely, the *Loewner* and the *optimal (frequency-limited) \mathcal{H}_2 frameworks*. The Loewner framework is recalled in its

general form, in section 3.1. The \mathcal{H}_2 model order dimension reduction methods is recalled in section 3.2, section 3.3 and section 3.4. In the following subsections, indices and exponents in eq. (6) and eq. (7) are dropped for simplicity.

3.1 Reminder of the Loewner framework

The main elements of the Loewner framework are recalled thereafter in the multi-input multi-output (MIMO) general square case. For a complete description readers may refer to [5, 24], and to [3] for insight in the rectangular case. Under mild considerations, the Loewner approach is a data-driven method aimed at building a rational descriptor **LTI** dynamical model \mathbf{H}^m of dimension m which interpolates given complex data, here generated by a model \mathbf{H} . Let us be given the left or row data, and the right or column data:

$$\left. \begin{array}{l} (\mu_j, \mathbf{l}_j^H, \mathbf{v}_j^H) \\ \text{for } j = 1, \dots, m \end{array} \right\} \text{ and } \left\{ \begin{array}{l} (\lambda_i, \mathbf{r}_i, \mathbf{w}_i) \\ \text{for } i = 1, \dots, m \end{array} \right. , \quad (8)$$

where $\mathbf{v}_j^H = \mathbf{l}_j^H \mathbf{H}(\mu_j)$ and $\mathbf{w}_i = \mathbf{H}(\lambda_i) \mathbf{r}_i$, with $\mathbf{l}_j \in \mathbb{C}^{n_y \times 1}$, $\mathbf{r}_i \in \mathbb{C}^{n_u \times 1}$, $\mathbf{v}_j \in \mathbb{C}^{n_u \times 1}$ and $\mathbf{w}_i \in \mathbb{C}^{n_y \times 1}$. The \mathbf{w}_i and \mathbf{v}_j are the complex measurement data at the points μ_j and λ_i , along the tangential directions \mathbf{l}_j and \mathbf{r}_i . In addition, let us assume that $\lambda_i \in \mathbb{C}$ and $\mu_j \in \mathbb{C}$ represent a set of distinct interpolation points $\{z_k\}_{k=1}^{2m} \subset \mathbb{C}$ which is split in two equal subsets as

$$\{z_k\}_{k=1}^{2m} = \{\mu_j\}_{j=1}^m \cup \{\lambda_i\}_{i=1}^m. \quad (9)$$

The method then consists in building the *Loewner* $\mathbb{L} \in \mathbb{C}^{m \times m}$ and *shifted Loewner* $\mathbb{L}_\sigma \in \mathbb{C}^{m \times m}$ matrices defined as follows, for $i = 1, \dots, m$ and $j = 1, \dots, m$:

$$\begin{aligned} [\mathbb{L}]_{j,i} &= \frac{\mathbf{v}_j^H \mathbf{r}_i - \mathbf{l}_j^H \mathbf{w}_i}{\mu_j - \lambda_i} = \frac{\mathbf{l}_j^H (\mathbf{H}(\mu_j) - \mathbf{H}(\lambda_i)) \mathbf{r}_i}{\mu_j - \lambda_i} \\ [\mathbb{L}_\sigma]_{j,i} &= \frac{\mu_j \mathbf{v}_j^H \mathbf{r}_i - \lambda_i \mathbf{l}_j^H \mathbf{w}_i}{\mu_j - \lambda_i} = \frac{\mathbf{l}_j^H (\mu_j \mathbf{H}(\mu_j) - \lambda_i \mathbf{H}(\lambda_i)) \mathbf{r}_i}{\mu_j - \lambda_i} \end{aligned} \quad (10)$$

Then, the model \mathbf{H}^m given by the following descriptor realisation,

$$\mathcal{S}^m : \begin{cases} E^m \delta \{ \mathbf{x}(\cdot) \} &= A^m \mathbf{x}(\cdot) + B^m \mathbf{u}(\cdot) \\ \mathbf{y}(\cdot) &= C^m \mathbf{x}(\cdot) \end{cases}, \quad (11)$$

where $E^m = -\mathbb{L}$, $A^m = -\mathbb{L}_\sigma$, $[B^m]_k = \mathbf{v}_k^H$ and $[C^m]_k = \mathbf{w}_k$ (for $k = 1, \dots, m$), and whose related transfer function

$$\mathbf{H}^m(\xi) = C^m (\xi E^m - A^m)^{-1} B^m, \quad (12)$$

interpolates \mathbf{H} at the given driving frequencies and directions defined in eq. (8), *i.e.* satisfies

$$\begin{aligned} \mathbf{l}_j^H \mathbf{H}^m(\mu_j) &= \mathbf{l}_j^H \mathbf{H}(\mu_j) \\ \mathbf{H}^m(\lambda_i) \mathbf{r}_i &= \mathbf{H}(\lambda_i) \mathbf{r}_i \end{aligned} \quad (13)$$

Remark 2 (About $\delta\{\cdot\}$ and ξ notations) In eq. (11), “ (\cdot) ” denotes the considered time-domain variable; this latter can either be “ (t) ” for continuous-time models ($t \in \mathbb{R}_+$) or “ $[q]$ ” for sampled-time models ($q \in \mathbb{Z}$). Similarly, in eq. (11) “ $\delta\{\cdot\}$ ” stands as the shift operator being either $\delta\{\mathbf{x}(t)\} = \dot{\mathbf{x}}(t)$ in the continuous-time case and $\delta\{\mathbf{x}(q)\} = \mathbf{x}[q+1]$ in the sampled one. With reference to eq. (12) ξ stands as the associated complex version being the Laplace variable $\xi = s$ in the continuous-time case and the forward shift $\xi = z$ in the sampled-time one.

Assuming that the number $2m$ of available data is large enough, then it has been shown in [24] that a minimal model \mathbf{H}^n of dimension $n < m$ that still interpolates the data can be built with a projection of eq. (11) provided that, for $k = 1, \dots, 2m$, where z_k are as in eq. (9),

$$\mathbf{rank}(z_k \mathbb{L} - \mathbb{L}_\sigma) = \mathbf{rank}([\mathbb{L}, \mathbb{L}_\sigma]) = \mathbf{rank}([\mathbb{L}^H, \mathbb{L}_\sigma^H]^H) = n. \quad (14)$$

In that case, let us denote by $Y \in \mathbb{C}^{m \times n}$ the matrix containing the first n left singular vectors of $[\mathbf{L}, \mathbf{L}_\sigma]$ and $X \in \mathbb{C}^{m \times n}$ the matrix containing the first n right singular vectors of $[\mathbf{L}^H, \mathbf{L}_\sigma^H]^H$. Then,

$$E^n = Y^H E^m X, A^n = Y^H A^m X, B^n = Y^H B^m, C^n = C^m X, \quad (15)$$

is a realisation of the model \mathbf{H}^n given as,

$$\mathbf{H}^n(\xi) = C^n (\xi E^n - A^n)^{-1} B^n, \quad (16)$$

with the same structure as eq. (12), embedding a *minimal McMillan degree* equal to $\mathbf{rank}(\mathbf{L})$. The quadruple $S^n : (E^n, A^n, B^n, C^n)$ is a descriptor realisation of \mathbf{H}^n . Note that if n in eq. (14) is greater than $\mathbf{rank}(\mathbf{L})$ then \mathbf{H}^n can either have a direct-feedthrough or a polynomial part. Reader may note that the number n of singular vectors composing Y and X used to project the system \mathbf{H}^n in eq. (15) may be decreased even further than n at the cost of approximate interpolation of the data. This allows for a trade-off between complexity of the resulting model and accuracy of the interpolation. Reader may note that Loewner extensions to some nonlinear systems exist, *e.g.* bilinear [6].

In this work we will always consider exact interpolation while the model reduction step, recalled in section 3.2, will be performed by (frequency limited) \mathcal{H}_2 -oriented interpolatory methods instead. These latter are detailed in a rather large framework in the following section 3.3 and section 3.4.

Remark 3 (Assumptions for model order reduction) *In what follows, we assume that \mathbf{H}^n is stable, strictly proper and has semi-simple poles. These assumptions can be theoretically removed but at the cost of a more complicated developments, not appropriate in our gust load setting. Indeed, any polynomial or constant terms, as highlighted in eq. (7), will be kept for simulation but discarded for control design, with a low if not null impact on the process.*

3.2 Model dimension reduction

Given the finite n -th order function \mathbf{H}^n equipped with a realisation defined by the quadruple $S^n : (E^n, A^n, B^n, C^n)$ given in eq. (15), the model reduction goal consists in constructing reduced r -th order ($r \ll n$) model

$$\hat{\mathcal{S}} : \begin{cases} \hat{E} \delta \{ \hat{\mathbf{x}}(\cdot) \} &= \hat{A} \hat{\mathbf{x}}(\cdot) + \hat{B} \mathbf{u}(\cdot) \\ \hat{\mathbf{y}}(\cdot) &= \hat{C} \hat{\mathbf{x}}(\cdot) \end{cases}, \quad (17)$$

where, $\hat{\mathbf{x}}(\cdot) \in \mathbb{R}^r$ is the reduced internal variables and $\hat{\mathbf{y}}(\cdot) \in \mathbb{R}^{n_y}$ is the approximated output, and where

$$\hat{E} \in \mathbb{R}^{r \times r}, \hat{A} \in \mathbb{R}^{r \times r}, \hat{B} \in \mathbb{R}^{r \times n_u} \text{ and } \hat{C} \in \mathbb{R}^{n_y \times r} \quad (18)$$

are constant matrices, such that the input output behaviour of $\hat{\mathbf{H}}$ defined as

$$\hat{\mathbf{H}}(\xi) = \hat{C} \left(\xi \hat{E} - \hat{A} \right)^{-1} \hat{B}, \quad (19)$$

is similar to \mathbf{H}^n , *i.e.* for the same input \mathbf{u} , the mismatch $\mathbf{y} - \hat{\mathbf{y}}$ is small in some sense.

3.3 Rational \mathcal{H}_2 approximation and reduction by interpolation

One way to find $\hat{\mathbf{H}}$ as in eq. (19) is to solve the so-called \mathcal{H}_2 model reduction problem², which aims at solving the following problem:

$$\hat{\mathbf{H}} = \arg \min_{\mathbf{G} \in \mathcal{H}_2} \|\mathbf{H}^n - \mathbf{G}\|_{\mathcal{H}_2}. \quad (20)$$

²Optimising through the \mathcal{H}_2 norm is relevant as it provides an upper bound on the worst case time-domain error in response to an input signal [18].

The most common approach to obtain the solution of eq. (20) is to work with the *first order necessary optimality conditions* which were developed in a series of papers, see *e.g.* [10, 37] for theoretical insight (see also [9] for existence and general properties). The *interpolation-based* approach revisited by a sequence of contributions [15, 38, 18] and resulting in an interpolatory problem is used here. In the case of semi-simple poles only (the case of higher order poles is presented in [39]), if $\hat{\mathbf{H}}$, equipped with a realisation $\hat{\mathcal{S}} : (\hat{E}, \hat{A}, \hat{B}, \hat{C})$ is a solution of the \mathcal{H}_2 approximation problem eq. (20), then

$$\begin{aligned} \mathbf{H}^n(\hat{\kappa}_l)\hat{\mathbf{b}}_l &= \hat{\mathbf{H}}(\hat{\kappa}_l)\hat{\mathbf{b}}_l \\ \hat{\mathbf{c}}_l^H \mathbf{H}^n(\hat{\kappa}_l) &= \hat{\mathbf{c}}_l^H \hat{\mathbf{H}}(\hat{\kappa}_l) \\ \hat{\mathbf{c}}_i^H \left. \frac{d\mathbf{H}^n}{d\xi} \right|_{\xi=\hat{\kappa}_l} \hat{\mathbf{b}}_l &= \hat{\mathbf{c}}_l^H \left. \frac{d\hat{\mathbf{H}}}{d\xi} \right|_{\xi=\hat{\kappa}_l} \hat{\mathbf{b}}_l \end{aligned} \quad (21)$$

where $[\hat{\mathbf{b}}_1, \dots, \hat{\mathbf{b}}_r]^H = R\hat{B}$ and $[\hat{\mathbf{c}}_1, \dots, \hat{\mathbf{c}}_r] = \hat{C}L$ and where $L \in \mathbb{C}^{r \times r}$ and $R \in \mathbb{C}^{r \times r}$ are the left and right eigenvectors associated to $\hat{\lambda}_l$, the eigenvalues of the (\hat{E}, \hat{A}) pair. Then, in the continuous-time case, $\hat{\kappa}_l = -\hat{\lambda}_l$ while in the discrete-time one, $\hat{\kappa}_l = 1/\hat{\lambda}_l$ ($l = 1, \dots, r$) [18, 11].

In [18], authors derive a Petrov-Galerkin like projection-based approach [40], accompanied with a fixed point algorithm, celebrated as **MIMO Iterative Rational Krylov Algorithm (MIMO IRKA)**, allowing reaching the optimality conditions eq. (21). The solution results in a procedure with a fairly cheap computational cost, embedding linear equation resolutions for which efficient methods are available [35, 22, 36, 19]. Details are skipped here but readers can also refer to the book [4] or monograph [29, Chap. 2] for practical details and numerical applications.

3.4 Rational frequency-limited \mathcal{H}_2 approximation and reduction by interpolation

Similarly to the above \mathcal{H}_2 model approximation problem, it might be interesting approximating over a frequency limited range $\Omega = [0, \omega]$ ($\omega \in \mathbb{R}_+$) only. This is the purpose of the *frequency-limited \mathcal{H}_2* , shortly $\mathcal{H}_{2,\Omega}$, approximation problem defined as [44, 27]:

$$\hat{\mathbf{H}} = \arg \min_{\mathbf{G} \in \mathcal{H}_\infty} \|\mathbf{H}^n - \mathbf{G}\|_{\mathcal{H}_{2,\Omega}}. \quad (22)$$

Interestingly, as in the seminal works of [18] treating the \mathcal{H}_2 objective, [41, Chap. 8] shown that this problem can also be recast as an interpolatory one.

However, unlike the \mathcal{H}_2 interpolation conditions, the frequency-limited ones do not involve directly the transfer functions \mathbf{H} and $\hat{\mathbf{H}}$ but irrational functions $\mathbf{T}_\omega^n(\mathbf{H})$ and $\hat{\mathbf{T}}_\omega(\hat{\mathbf{H}})$, parametrised by \mathbf{H} and $\hat{\mathbf{H}}$. Here again, these functions should match at images of the poles of the reduced-order model (see details in [41, Chap. 8]).

As it, these interpolatory conditions are difficult to practically exploit. Indeed, no Krylov-like subspace have been clearly identified yet. Consequently, a **MIMO IRKA** like procedure as in [18] is not straightforward to develop³. So far, this $\mathcal{H}_{2,\Omega}$ problem has been attacked using the **DARPO** procedure [41, Chap. 8], a descent algorithm, and **FL-ISTIA** procedure [43], involving frequency-limited gramian, taking advantage of a subset of the interpolation conditions eq. (21). In the remaining of the paper, we will consider the **FL-ISTIA** procedure developed in [43].

4 Interpolatory-driven aero-servoelastic aircraft gust load oriented reduced modelling

Back to our GLA problem, we will now invoke the interpolatory results of section 3 to construct an appropriate control-oriented model for the GLA control design, simulation and analysis. The

³Note that in [28], a similar procedure achieving first order \mathcal{H}_2 optimality with interpolatory conditions with an input-output delayed **LTI** model has been developed.

following section 4.2 and section 4.3 successively describe the exact continuous-time rational approximation and frequency-limited model order reduction of the aeroelastic business jet aircraft models. The reason for these successive sections are justified in section 4.1. Numerical results are presented in section 4.4.

4.1 Models limitations for control purpose

This BizJet use-case is described by models defined as eq. (6) in state-space form $\{\mathcal{S}_i\}_{i=1}^{n_s}$ and eq. (7) in its transfer form $\{\mathbf{H}_i\}_{i=1}^{n_s}$. These relations are not appropriate to manipulate in a control design objective for the following reasons: (i) the internal vector dimension of each model $\mathcal{S}^{(i)}$ is large (i.e. $N_i \approx 300$), leading to medium-scale matrices and a computational burden inappropriate with the control design; (ii) the presence of internal delays renders the model irrational and results in an infinite number of eigenvalues, for which dedicated tools exist but are complex to manipulate in an industrial context; (iii) the $E^{(i)}$ matrix being rank defective, the computational tools are not always appropriate and transferable in an applicative context.

4.2 BizJet aircraft rational and polynomial approximation

The first step of the process consists in replacing each infinite⁴ dimensional model $\{\mathbf{H}_i\}_{i=1}^{n_s}$ eq. (7) by a finite order rational n_i -th order one, $\{\mathbf{H}_i^{n_i}\}_{i=1}^{n_s}$ ($i = 1, \dots, n_s$). By considering each n_s continuous-time model of the considered GLA use-case described in section 1, one can apply the rational approximation by interpolation using the method recalled in section 3.1. Then one obtains a set of n_s continuous-time rational approximated models $\{\mathbf{H}_i^{n_i}\}_{i=1}^{n_s}$ as eq. (16) equipped with realisation $\{\mathcal{S}_i^{n_i}\}_{i=1}^{n_s}$ with matrices as eq. (15). Note that each of the n_s models may have a different dimension n_i ; this latter being automatically computed by the rank condition given in eq. (14). Here, as the original models eq. (7) are given in continuous-time, it is convenient to select the interpolation points along the imaginary axis. In our case, for all configurations, the interpolating points eq. (9) have been selected as follows :

$$\{z_k\}_{k=1}^{2m} = \underbrace{\{\omega_j, -\omega_j\}_{j=1}^{m/2}}_{\{\mu_j\}_{j=1}^m} \cup \underbrace{\{\nu_i, -\nu_i\}_{i=1}^{m/2}}_{\{\lambda_i\}_{i=1}^m}, \quad (23)$$

where $\omega_j, \nu_i \in \mathbb{R}_+$ are the pulsations at which one evaluates each transfer $\{\mathbf{H}_i\}_{i=1}^{n_s}$, with $m = 1000$. In our application ω_j and ν_i are selected to be logarithmically spaced from 10^{-2} to 10^3 . This choice allows to focus on the frequency range of interest. Indeed, in the case of irrational models, the method is efficient for interpolation but not necessary for extrapolation.

In addition, as the stability of the obtained rational model $\{\mathbf{H}_i^{n_i}\}_{i=1}^{n_s}$ is not guaranteed by the Loewner interpolatory procedure, a *post stabilisation* is performed using the procedure presented in [21]. This latter consists in projecting the rational models $\{\mathbf{H}_i^{n_i}\}_{i=1}^{n_s}$ onto its closest stable subset, here using the \mathcal{H}_∞ -norm, leading to a stable model of the same dimension. Mathematically, given a realisation \mathcal{S} associated to $\mathbf{H} \in \mathcal{L}_\infty$, one aims at finding $P_\infty(\mathbf{H}) \in \mathcal{H}_\infty$ such that,

$$P_\infty(\mathbf{H}) = \arg \inf_{\mathbf{G} \in \mathcal{H}_\infty} \|\mathbf{H} - \mathbf{G}\|_{\mathcal{H}_\infty}. \quad (24)$$

Technical details and assumption can be found in [21]. Each model now share a rational structure as the one given in eq. (17)-eq. (19), and is now stable and of finite order n_i , for $i = 1, \dots, n_s$. Note that here, the stability enforcement is performed since one knows that original models are structurally and physically stable. At this point, the delay difficulty is removed and traded with rational order model n_i automatically determined by eq. (14).

Remark 4 (About a Padé delay approximation) *It can be appealing to replace the delays with a Padé approximation, which preserves the gain but modifies the phase. Indeed, while this is*

⁴These models, embedding a state-space of order N_i are of infinite dimension due to the internal delays, leading to infinite number of eigenvalues.

classically performed in many applications, it is, to the authors experience, not the best way to deal with delays, especially in flexible structure models where phase vary a lot. In addition, the use of Padé will drastically increases the model internal vector. Although it may not be a problem, Padé usually results in poor accuracy, specifically in flexible structure, affecting the phase. Instead, we prefer rational multi-point interpolation while Padé may be viewed as an interpolation at higher order, at zero.

4.3 BizJet aircraft control-oriented model reduction

As a second step, and rooted on $\{\mathbf{H}_i^{n_i}\}_{i=1}^{n_s}$, the obtained continuous-time rational models, one now invokes again the *interpolatory framework* for a dimension reduction. Now we follow the approach detailed in section 3.4 to reduce the model over a frequency-limited range. For the considered application, and in view of control design, it is important to reduce as much as possible the model while staying representative. Indeed, as the controller designed later is a solution of an optimisation problem, the simpler the model is, the more accurate and faster the optimisation is.

In addition, as the GLA function should act in a given frequency range without altering the flight control laws, it is relevant to reduce the model over a frequency limited range $[0, \omega]$, only (where $\omega \in \mathbb{R}_+$). **FL-ISTIA** process [43] being also a fixed point procedure, its initialisation is done by selecting starting interpolating points as follows:

$$\begin{aligned} \{\hat{\kappa}^{(0)}\}_{k=1}^r &= \{\omega_k, -\omega_k\}_{k=1}^{r/2} && \text{if } r \text{ is even} \\ \{\hat{\kappa}^{(0)}\}_{k=1}^r &= \{\omega_k, -\omega_k\}_{k=1}^{\lfloor r/2 \rfloor} \cup \omega_0 && \text{if } r \text{ is odd} \end{aligned} \quad , \quad (25)$$

where $0 < \omega_k < \omega$ and $\omega_0 < \omega$. The interpolatory conditions presented in eq. (21) can also be partially ensured.

4.4 Application to the BizJet models

As an illustration, fig. 2 compares the frequency and phase responses from the gust input to a wing root bending moment of the original irrational model \mathbf{H}_7 with its rational approximations $\mathbf{H}_7^{n_7}$ and frequency-limited reduced model $\hat{\mathbf{H}}_7$ for one single configuration point. Sigma plot and mismatch errors are also reported in fig. 3. All other cases are similarly obtained.

With reference to fig. 2 and fig. 3, the following comments can be done. First, the rational approximation, satisfying the tangential interpolatory conditions eq. (13), allows to accurately capture the descriptor delayed model eq. (7) gain, phase and sigma, with a simple rational model (here for the 7-th use-case, $n_7 = 211$) of the form eq. (16). Note that the projection [21] performed afterward to force the model to be stable let the matching accurate enough. Second, the frequency-limited order reduction still preserves a good matching in the considered frequency range, with a rational model as eq. (19) of dimension $r = 30$ only. Analysing the bottom frame of fig. 3, the $\mathbf{H}_7 - \mathbf{H}_7^{n_7}$ (unstable) mismatch is close to machine precision up to the upper frequency limit ω ; this is caused by the tangential directions which may produce less accurate transfers. When projecting to obtain a stable model, the $\mathbf{H}_7 - \mathbf{H}_7^{n_7}$ (stable) mismatch results in a loss of accuracy, traded with the stability property. The reduced model $\hat{\mathbf{H}}_7$ clearly is accurate below the upper frequency bound, and can be considered as simple but accurate enough for GLA control design.

5 Interpolatory-driven sampled-time feedback gust load alleviation function computation

Given the continuous-time reduced order models $\{\hat{\mathbf{H}}_i\}_{i=1}^{n_s}$, we are now ready to design the GLA control function. As this control law has to be implemented on a on-board computer sampled with a fixed step time $h \in \mathbb{R}_+$, a sampled-time (or discrete-time) controller is sought. In the rest of this section, we first present the context of discrete-time control design in section 5.1. Then, based on the continuous-time reduced models $\{\hat{\mathbf{H}}_i\}_{i=1}^{n_s}$, the continuous-time synthesis of \mathbf{K} , in

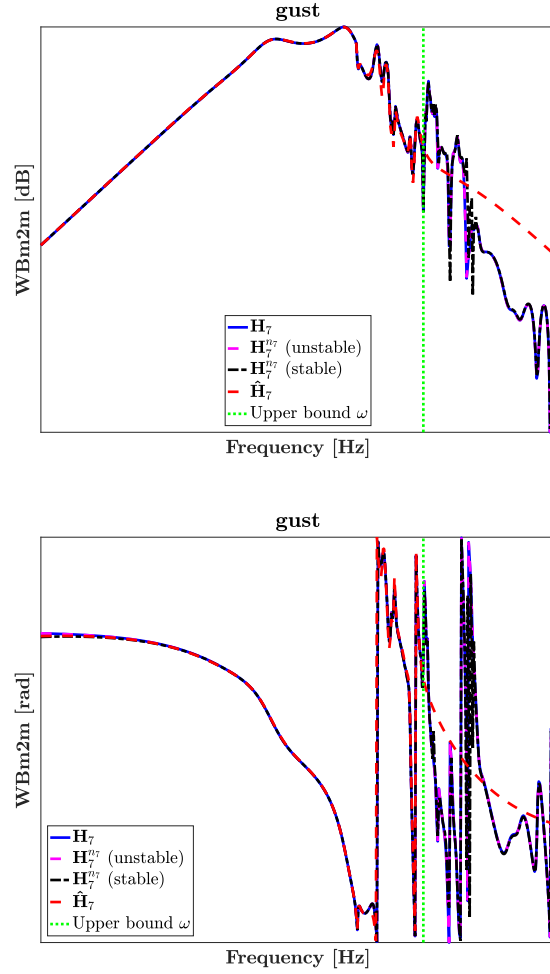


Figure 2: Gain (top) and phase (bottom) frequency responses of one transfer from gust to a wing root bending moment. The original model \mathbf{H}_7 (solid blue), the approximated and approximated plus projected stable models \mathbf{H}_7^{n7} (dashed magenta dash dotted black, respectively) and the reduced order model $\hat{\mathbf{H}}_7$ with dimension $r = 30$. Upper bound of the reduction frequency band is materialised by the vertical green dashed line.

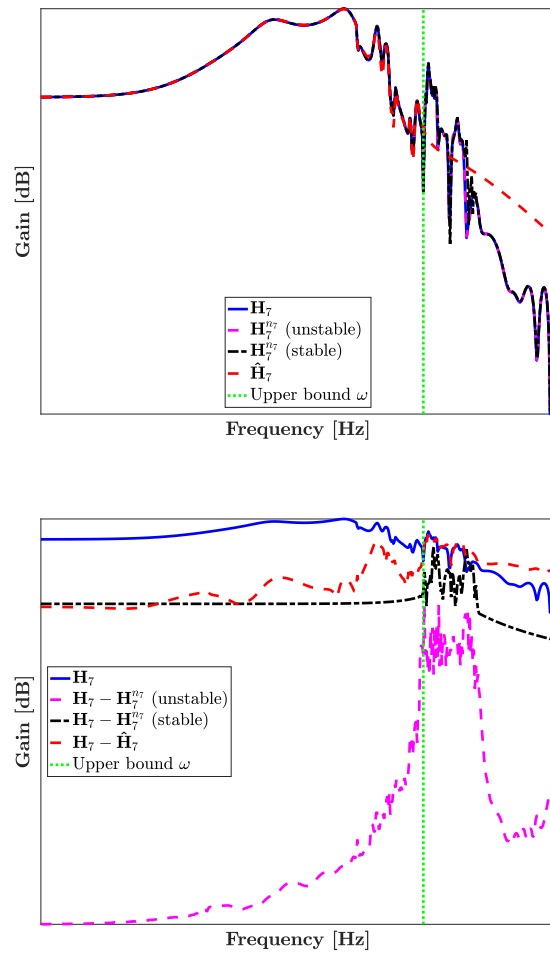


Figure 3: Gain (top) and gain error (bottom) of the singular frequency responses of the different models.

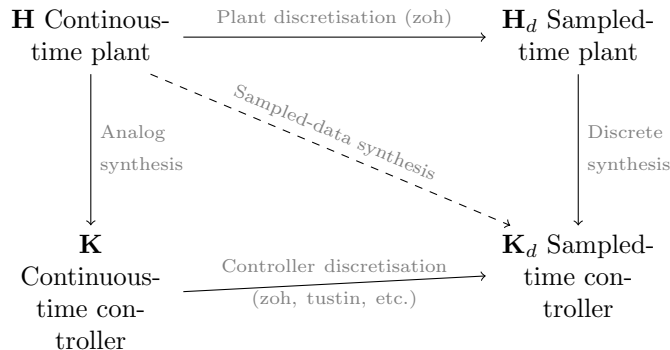


Figure 4: Different paths to design a discrete control-law \mathbf{K}_d from an analog plant \mathbf{H} .

the continuous-time \mathcal{H}_∞ -norm, is briefly exposed in section 5.2. Then, section 5.3 exposes the discretisation problem, which is then solved in the *new interpolatory framework* in section 5.4, leading to algorithm 1.

5.1 Preliminary words on discrete and continuous-time control design

In dynamical systems and control theory, the continuous-time and discrete-time domains coexist. While most of the tools available in one domain have a counterpart in the other, it is not unusual that a specific application requires to switch from one domain to the other. In particular, in the considered GLA control-oriented application, engineers start from a continuous-time physical model set $\{\mathbf{H}_i\}_{i=1}^{n_s}$, simplified by a reduced continuous-time one $\{\hat{\mathbf{H}}_i\}_{i=1}^{n_s}$. The latter is then used for the design of the GLA control law. To this aim, as illustrated schematically in fig. 4, three approaches can be conducted: (i) one may discretise the analog plants $\{\mathbf{H}_i\}_{i=1}^{n_s}$ and then design a discrete control-law \mathbf{K}_d with the same sampling period h , (ii) conversely, one may design an analog control-law \mathbf{K} and then discretise it, (iii) or, using dedicated techniques from sampled-data systems theory (see *e.g.* [13, Chap. 12-13]), one may directly synthesise \mathbf{K}_d from $\{\mathbf{H}_i\}_{i=1}^{n_s}$.

While the direct nature of the latter method (iii) is appealing, it requires dedicated theoretical and numerical tools that are not as widespread as usual ones, especially in the industry where this approach would require their whole control design and analysis process to be rethought. For these reasons, one focuses here on the indirect methods that remain of practical interest, and more specifically on the continuous controller, followed by a discretisation. Performing in the other ways, *i.e.* discretising the model and then synthesising the controller would lead to an inaccurate model response due to the low frequency sampling imposed by the on-board computer.

For both indirect approaches, a discretisation step is required. This may have a detrimental impact with respect to the expected dynamical behaviour, especially if hard computational constraints on the sampling period h are imposed by the technology, which may happen with critical systems. In that context, the availability of an efficient discretisation method is of particular interest. Here, an approach based on the *Loewner interpolatory framework* [24], recalled in section 3.1, is used. It offers an interesting alternative to usual discretisation processes as it enables to reach a better frequency and time-domain matching with the continuous-time description. Before detailing this approach, for sake of completeness, section 5.2 briefly presents the continuous-time GLA controller design.

5.2 Preliminary continuous-time GLA controller design

In the considered application, as the objective is to attenuate a worst case amplification, the \mathcal{H}_∞ -norm minimisation framework is clearly tailored. This optimisation method is then used, on the basis of the reduced continuous-time model representation. Note that this framework, and linear ones, are largely used and mastered in aeronautical applications [26, 30, 1], and is preferred here

also. Being given the reduced continuous-time models $\{\hat{\mathbf{H}}_i\}_{i=1}^{n_s}$, the continuous-time controller \mathbf{K} , mapping outputs \mathbf{y} to control inputs \mathbf{u} , as interconnected on fig. 1, is obtained by solving the following \mathcal{H}_∞ -norm problem, for $i = 1, \dots, n_s$,

$$\mathbf{K} = \arg \min_{\tilde{\mathbf{K}} \in \mathcal{K} \subseteq \mathcal{H}_2} \|\mathcal{F}_l(\mathbf{G}(\hat{\mathbf{H}}_i), \tilde{\mathbf{K}})\|_{\mathcal{H}_\infty}, \quad (26)$$

where $\mathbf{G}(\hat{\mathbf{H}}_i) \in \mathcal{H}_\infty$ is the so-called generalised plant involving the input and output weight functions (not detailed here as out of the scope) and the reduced order models. Moreover $\mathcal{F}_l(\cdot, \cdot)$ denotes the lower fractional operator. The control objective thus consists in finding the locally-optimal continuous-time controller \mathbf{K} , such that eq. (26) is solved, *i.e.* such that the \mathcal{H}_∞ -norm of the $\mathcal{F}_l(\mathbf{G}(\hat{\mathbf{H}}_i), \mathbf{K})$ loop, mapping exogenous inputs \mathbf{w} to performance output \mathbf{z} (here being the loads and some tracking objectives), is minimised. In the considered case, one seeks this controller such that it belongs to a subset $\mathcal{K} \subseteq \mathcal{H}_2$, reducing the controller search space to reduced order structures without direct feed-through, avoiding issues for industrial implementation. The problem is solved by the routine developed by the authors of [7] and results in a stable moderate n_c -th order **LTI** continuous-time controller \mathbf{K} .

5.3 Controller discretisation problem statement and discretisation error derivation

Being given the linear continuous-time controller \mathbf{K} , the objective here is to determine, for a fixed time-step $h \in \mathbb{R}_+$, a discrete-time controller represented by the recurrence state-space equation,

$$\mathcal{C}_d : \begin{cases} \mathbf{x}_d[q+1] &= A_d \mathbf{x}_d[q] + B_d \mathbf{y}_d[q] \\ \mathbf{u}_d[q] &= C_d \mathbf{x}_d[q] + D_d \mathbf{y}_d[q] \end{cases} \quad (27)$$

where $\mathbf{x}_d[q] \in \mathbb{R}^{n_d}$, $\mathbf{u}_d[q] \in \mathbb{R}^{n_u}$, $\mathbf{y}_d[q] \in \mathbb{R}^{n_y}$ are the internal variables, sampled control and measurements signals respectively. One seeks for eq. (27) such that (i) its associated transfer function $\mathbf{K}_d(z) = C_d(zI_{n_d} - A_d)^{-1}B_d + D_d$ is stable, *i.e.* $\mathbf{K}_d \in \mathcal{H}_\infty(\overline{\mathcal{D}})$, and (ii) the input-output behaviour of \mathbf{K} is well reproduced by \mathbf{K}_d up to the Nyquist frequency. While discretisation methods such as the bilinear (Tustin) are clearly able to build a discrete-time model satisfying (i) the input-output behaviour may be quite far from the original one when h is too large. Here, a method is proposed to build such a model by first using the *Loewner framework* to interpolate a specific set of frequency data and then, similarly to section 4.2, projecting the resulting model onto the stable subspace $\mathcal{H}_\infty(\overline{\mathcal{D}})$ to enforce sampled-time controller stability.

5.3.1 Measure of the discretisation error

Quantifying the error induced by the discretisation of \mathbf{K} is not trivial due to the incompatible nature with \mathbf{K}_d that prevents from interconnecting the two systems. Indeed, one cannot just consider $\mathbf{K} - \mathbf{K}_d$. Digital to analog converters are required. For a sampling time $h \in \mathbb{R}_+$, the latter are modelled here as the ideal sampler S and holder H . Then, the error system is given by the interconnection of fig. 5 where discrete-time signals are represented by dashed lines. Such an interconnection of continuous and discrete time models is called a *Sampled-data System (SD)*.

The controller $\tilde{\mathbf{K}} = S\mathbf{K}_dH$ is no longer **LTI** but h -periodic and consequently, so is the error $\mathbf{K} - \tilde{\mathbf{K}}$ for which usual system norms cannot directly be applied. This problem has been addressed in the literature for direct **SD** synthesis (see *e.g.* [8, 13] and references therein). The recurring idea is to use continuous lifting to transform a periodic system into a discrete-time **LTI** model with infinite input and output spaces on which equivalent \mathcal{H}_2 or \mathcal{H}_∞ norms can be defined.

While this framework appears well suited to evaluate $\mathbf{K} - \tilde{\mathbf{K}}$, the infinite dimensionality of the lifted model makes it quite technical. That is why here, a more straightforward approach based on the *frequency characterisation of the discretisation error* formulated in [13, section 3.5] is considered instead. For that purpose, models for the ideal sampler and holder are recalled in section 5.3.2 and the frequency error is presented in section 5.3.3⁵.

⁵Note that in [13], the authors use the λ -transform while here, one considers the z -transform, the sign of the

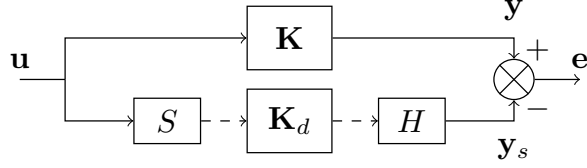


Figure 5: Interconnection for the measurement of the discretisation error between G and G_d .

5.3.2 Ideal sampler and holder

Let us consider a continuous-time signal $v(t)$ and the sampling period h . The ideal sampler S transforms $v(t)$ into a discrete sequence $v_d[q]$ such that,

$$v_d[q] = v(qh), \quad q \in \mathbb{Z}. \quad (28)$$

As shown in [13, Lemma 3.3.1], the Fourier transforms $\bar{v}_d = \mathcal{F}(v_d)$ and $\bar{v} = \mathcal{F}(v)$ are linked as follows,

$$\bar{v}_d(e^{i\omega h}) = \frac{1}{h} \sum_{q \in \mathbb{Z}} \bar{v}(i\omega + iq\omega_s), \quad (29)$$

where $\omega_s = 2\pi/h$ is the sampling frequency. Equation eq. (29) highlights the frequency aliasing phenomena since all the multiples of the sampling frequency are indistinguishable in the output. Note that the sampling operator S is not bounded for any signal in $\mathcal{L}_2(\mathbb{R})$ as shown in [12]. To be bounded, the input signal v must be restricted to the class of band-limited $\mathcal{L}_2(\mathbb{R})$ signals or it must be filtered by a finite-dimensional stable and strictly causal system, *i.e.* an anti-aliasing filter.

Similarly, the holder H transforms a sequence $v_d[q]$ into a continuous-time signal $v(t)$ such that,

$$v(t) = v_d[q], \quad qh \leq t < (q+1)h. \quad (30)$$

The impulse response of the holder can be defined as the difference of two unit steps delayed by h . Let

$$R(s) = \frac{1 - e^{-sh}}{sh} \quad (31)$$

be the associated transfer function. Then, as shown in [13, Lemma 3.3.2], the Fourier transforms of v and v_d are linked as follows,

$$\bar{v}(i\omega) = hR(i\omega)\bar{v}_d(e^{i\omega h}). \quad (32)$$

Back to fig. 5, coupling equations (29) and (32) enables to express the frequency-domain relationship between \mathbf{u} and \mathbf{y}_s (for $|\omega| < |\omega_s|$),

$$\bar{\mathbf{y}}_s(i\omega) = R(i\omega)\mathbf{K}_d(e^{i\omega h}) \sum_{k \in \mathbb{Z}} \bar{\mathbf{u}}(i\omega + ik\omega_s). \quad (33)$$

5.3.3 A frequency domain error

Using equation (33), one can express the frequency-domain relationship between \mathbf{u} and the discretisation error $\mathbf{e} = \mathbf{y} - \mathbf{y}_s$ from Figure 5 as

$$\bar{\mathbf{e}}(i\omega) = \mathbf{K}(i\omega)\bar{\mathbf{u}}(i\omega) - R(i\omega)\mathbf{K}_d(e^{i\omega h}) \sum_{k \in \mathbb{Z}} \bar{\mathbf{u}}(i\omega + ik\omega_s). \quad (34)$$

exponential in the Fourier transforms of discrete signal is thus modified.

Assuming that \mathbf{u} is band-limited, *i.e.* that $\bar{\mathbf{u}}(\omega) = 0$ for $|\omega| > \omega_s/2 = \omega_N$, then (34) becomes

$$\bar{\mathbf{e}}(\omega) = (\mathbf{K}(\omega) - R(\omega)\mathbf{K}_d(e^{j\omega h})) \bar{\mathbf{u}}(\omega). \quad (35)$$

This readily suggests to consider

$$e_\infty(\mathbf{K}, \mathbf{K}_d) = \max_{\omega < \omega_N} |\mathbf{K}(\omega) - R(\omega)\mathbf{K}_d(e^{j\omega h})|, \quad (36)$$

to quantify the discretisation error. This frequency-domain characterisation of the error inspired the discretisation process presented in the next section. For the **MIMO** case, the absolute value in (36) may be replaced by the 2-norm.

5.4 Application of the Loewner framework for discretisation

Now we are ready to describe the *interpolatory driven discretisation process* allowing to get \mathbf{K}_d from the continuous-time controller \mathbf{K} .

5.4.1 Principle

Being given the considerations of section 5.3, let us consider the transfer function of the controller $\mathbf{K} \in \mathcal{H}_\infty$ to be discretised at the sampling time h . Building a n_c -th order discrete-time model \mathbf{K}_d that matches the input-output behaviour of \mathbf{K} , the frequency-domain characterisation of the discretisation error eq. (36) suggests that \mathbf{K}_d must be such that

$$R(\omega)\mathbf{K}_d(e^{j\omega h}) = \mathbf{K}(\omega), \quad (37)$$

for $|\omega| < \omega_N$. Equation eq. (37) represents an infinite number of interpolation conditions that may be approximated by sampling the interval $[0, \omega_N]$ such that for $k = 1, \dots, 2m$,

$$R(\omega_k)\mathbf{K}_d(e^{j\omega_k h}) = \mathbf{K}(\omega_k). \quad (38)$$

Such a model can be built by applying the *Loewner interpolation* framework recalled in section 3.1 to the following set of frequency data,

$$\{e^{j\omega_k h}, R(\omega_k)^{-1}\mathbf{K}(\omega_k)\}_{k=1}^{2m}, \quad (39)$$

where $e^{j\omega_k h}$ are the new interpolating points and $R(\omega_k)^{-1}\mathbf{K}(\omega_k)$ the new function to evaluate. With reference to eq. (8) and eq. (9) $e^{j\omega_k h}$ are the z_k . Then by splitting them in the same ways, $R(\omega_k)^{-1}\mathbf{K}(\omega_k)$ represents the couple \mathbf{v}_j^H and \mathbf{w}_i . Following the notations of section 3.1, one obtains the m -th order \mathbf{K}_d^m controller that can be lowered without loss of interpolatory accuracy to \mathbf{K}_d^n ($n < m$). Obviously, should the order n_c be lower than the McMillan order n of the exact interpolating model given by the Loewner approach, then the interpolation conditions (38) will not be perfectly satisfied, but the controller will keep its original dimension.

5.4.2 About the stability of the discretised model

The Loewner framework does not ensure the stability of the resulting interpolated model, here controller. Therefore, even if $\mathbf{K} \in \mathcal{H}_2$ (or \mathcal{H}_∞), the transfer function \mathbf{K}_d obtained via the process described above may not lie in $\mathcal{H}_\infty(\overline{\mathcal{D}})$ which is a major drawback in comparison to stability preserving discretisation schemes like the bilinear (Tustin) or backward ones.

To overcome this issue, one can apply the same process as in [17] and as performed in section 4.2 (in the continuous-time). It consists in projecting the unstable model \mathbf{K}_d onto $\mathcal{H}_\infty(\overline{\mathcal{D}})$ so that the \mathcal{L}_∞ norm between \mathbf{K}_d and its projection is minimised. This is the so-called Nehari problem for which solutions have been given in the continuous-time domain [16] and in the discrete-time domain, see *e.g.* [23].

Algorithm 1 Loewner-driven discretisation

Require: A continuous-time model $\mathbf{K} \in \mathcal{H}_\infty(\mathbb{C}_+)$, a sampling time $h > 0$, an upper bound \bar{n} of the desired order and a number m of interpolation points.

- 1: Sample the interval $]0, \omega_N[$ in $2m$ points ω_k
 - 2: Evaluate $R(i\omega_k)^{-1}\mathbf{K}(i\omega_k)$
 - 3: Apply Loewner to the data-set (39) to get a first model \mathbf{K}_d^m that matches all the data and get the underlying minimal McMillian order n
 - 4: Set $r = \min(n, \bar{n})$
 - 5: Reduce \mathbf{K}_d^m to \mathbf{K}_d^r using any interpolation method
 - 6: Project \mathbf{K}_d^r onto a stable subspace, *i.e.* compute the n_c -th order $\mathbf{K}_d = P_\infty(\mathbf{K}_d^r)$
 - 7: **return** the model $\mathbf{K}_d \in \mathcal{H}_\infty(\overline{\mathcal{D}})$ of order $n_c \leq r \leq \bar{n}$
-

Let us denote by P_∞ this projection operator so that if $\mathbf{K}_d \in \mathcal{L}_\infty(\partial\mathcal{D})$ then $P_\infty(\mathbf{K}_d) \in \mathcal{H}_\infty(\overline{\mathcal{D}})$ minimises

$$\|\mathbf{K}_d - P_\infty(\mathbf{K}_d)\|_{\mathcal{L}_\infty}. \quad (40)$$

Note that in the sampled-time case, the order of $P_\infty(\mathbf{K}_d)$ depends on the number of unstable poles of \mathbf{K}_d and is lower than n_c when \mathbf{K}_d is unstable. In particular, if \mathbf{K}_d has n_+ stable and n_- unstable poles and that m is the multiplicity of the largest unstable Hankel singular value, then $P_\infty(\mathbf{K}_d)$ has order $n_+ + n_- - m$ (see [23]). To avoid this issue and for a numerically more robust approach, sub-optimal projection methods may alternatively be considered (see *e.g.* [21]).

Remark 5 (Alternative approach) *A similar problem can be considered using the \mathcal{L}_2 -norm and is actually much easier to solve considering the decomposition $\mathcal{L}_2(\partial\mathcal{D}) = \mathcal{H}_2(\mathcal{D}) \oplus \mathcal{H}_2(\overline{\mathcal{D}})$. The solution is simply obtained by discarding the unstable part of the model. However this solution has generally a greater impact on the frequency behaviour of the model which is not desirable here.*

5.4.3 Loewner-driven discretisation

The Loewner-driven discretisation process of the controller is summarised in algorithm 1. The following comments can be added:

- the reduction step from \mathbf{K}_d^m to \mathbf{K}_d^r (step 5) may also be achieved by standard model approximation techniques as the one presented in section 3.3 or, more interestingly, using the frequency-limited version of section 3.4. Then \mathbf{K}_d^r should be projected on $\mathcal{H}_\infty(\overline{\mathcal{D}})$ and finally a stability preserving model reduction method could be used to obtain \mathbf{K}_d .
- As both \mathbf{K}_d^r and \mathbf{K}_d are easily available during the process, $\|\mathbf{K}_d^r - \mathbf{K}_d\|_{\mathcal{L}_\infty}$ can be evaluated to get an estimation of the discretisation error $e_\infty(\mathbf{K}, \mathbf{K}_d)$ in (36).
- Consequently, when $n_c = r$, computing $\|\mathbf{K}_d^r - \mathbf{K}_d\|_{\mathcal{L}_\infty}$ gives insight on whether the maximal allowed order \bar{n} is enough to ensure a low error.
- If \mathbf{K}_d^r is unstable, then step 6 leads to a loss of order (see section section 5.4.2). Therefore, when $n_c < r$ (which is likely to happen⁶), r should be increased above \bar{n} so that $P_\infty(\mathbf{K}_d)$ is of order \bar{n} thus avoiding any loss of accuracy.

It should also be noted that algorithm 1 does not exploit the state-space structure of \mathbf{K} and only requires frequency data from it. Therefore, as presented in the preliminary work [42], the approach may be applied to a wider class of models than just those described by a state-space realisation. algorithm 1 is applied on the obtained continuous-time GLA controller. The obtained sampled-time controller sigma plot is shown in fig. 6, comparing the responses of the continuous-time controller \mathbf{K} interconnected with a holder, with different sampled controllers obtained with different methods (but same order n_c). In addition fig. 7 reports the gain and phase mismatches of the different sampled controllers.

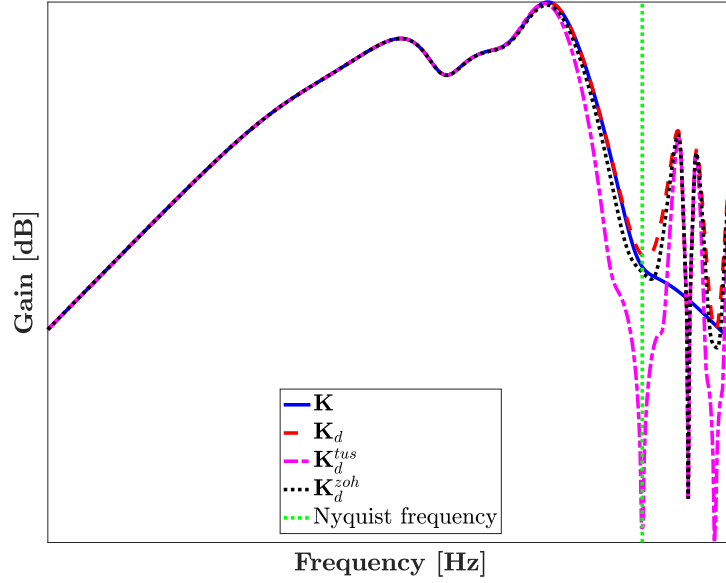


Figure 6: Comparison of the sigma plot of different controllers: the continuous-time one \mathbf{K} with holder (solid blue), the discrete-time obtained with backward method \mathbf{K}_d^{zoh} (dotted black), the discrete-time obtained with bilinear method \mathbf{K}_d^{tus} (dash dotted magenta) and the discrete-time obtained with the interpolatory method method \mathbf{K}_d (dashed red).

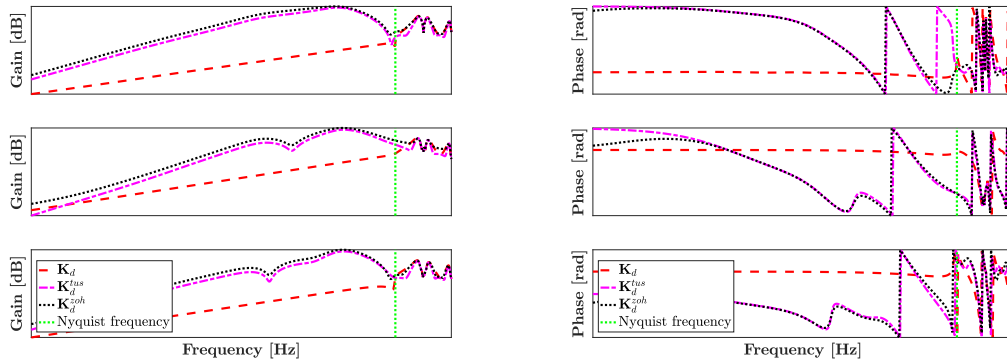


Figure 7: Gain (left) and phase (right) errors: comparison of the Bode plot of different sampled controllers with the continuous-time one \mathbf{K} with holder. The discrete-time obtained with backward method \mathbf{K}_d^{zoh} (dotted black), the discrete-time obtained with bilinear method \mathbf{K}_d^{tus} (dash dotted magenta) and the discrete-time obtained with the interpolatory method method \mathbf{K}_d (dashed red).

With reference to fig. 6 and fig. 7, one may observe that the obtained \mathbf{K}_d well reproduces the original controller \mathbf{K} behaviour up to the Nyquist frequency, while the bilinear approach \mathbf{K}_d^{tus} tends to compress the responses, both bilinear and backward importantly modify the phase. This accurate restitution obtained by \mathbf{K}_d is first justified by embedding the holder model in the control law before discretisation. Second, as the complete controller is now delayed, once again the interpolatory framework is adapted and thus outperforms the classic ones. More important effects on the closed-loop will be presented in the conclusion section 6.

6 Conclusions

In this paper, a complete end to end approach for the construction of a GLA control function has been presented, applied and implemented on a real-life generic BizJet aircraft use-case simulator. As a conclusion to this paper, section 6.1 presents the obtained performances when plugging the discrete-time controller in the complete industrial simulator including the time-delayed continuous-time model (hundreds of simulations are performed). As the proposed design scheme can be readily applied to any linear dynamical systems and not only aircraft control, in section 6.2 we summarise the main methodological contributions and potential improvement axes.

6.1 BizJet aircraft GLA function performances

The main objective of GLA is to reduce the so-called load envelope, *i.e.* the load amplification along the wing span in response to a gust signal family usually considered by aircraft manufacturers and authorities. This alleviation feature is presented on fig. 8, for different discretised controllers, with the same dimension and sampling-time value h .

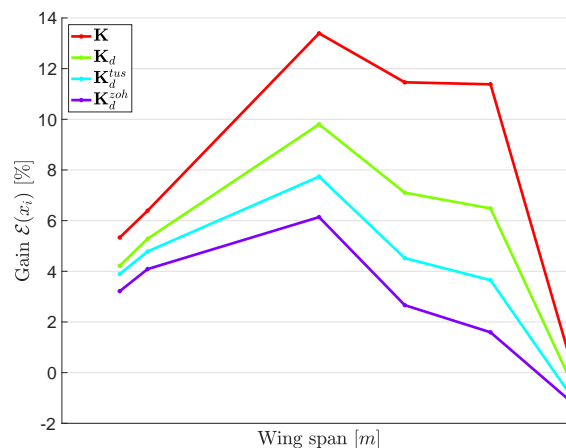


Figure 8: Gust load attenuation envelope gain $\mathcal{E}(x_i)$ resulting to the interconnection presented in fig. 1 for different GLA controllers: the continuous-time one \mathbf{K} (red), the discrete-time obtained with backward method \mathbf{K}_d^{zoh} (purple), the discrete-time obtained with bilinear method \mathbf{K}_d^{tus} (cyan) and the discrete-time obtained with the interpolatory method method \mathbf{K}_d (green).

While, the “optimal” gust load alleviation level obtained by the continuous-time controller \mathbf{K} leads to attenuation between 6 to 13% (except at the wing tip, where the loads are very small), the sampled-time versions with a sampling value h fixed by the available on-board computer clearly deteriorate the performances. Still, depending on the discretisation method, one clearly

⁶Indeed, one tries to approximate data coming from an infinite dimensional model by a rational one. A large order r is generally required to achieve an exact interpolation.

observes an important gain when using the proposed discretisation approach of algorithm 1, with respect to the standard ones. It is to be noted that every additional percent may represent hundreds of kilograms of mass reduction, and thus of aircraft global consumption. In addition, as a standard industrial requirement, the proposed load alleviation should not result in a change of flight performances. This is ensured by the control design and illustrated on fig. 9 where the normalised load factor variation in response to an elevator request $\delta_{mc}^*(t)$, results in similar behaviours with and without the GLA function, which fulfils the industrial process and constraints.

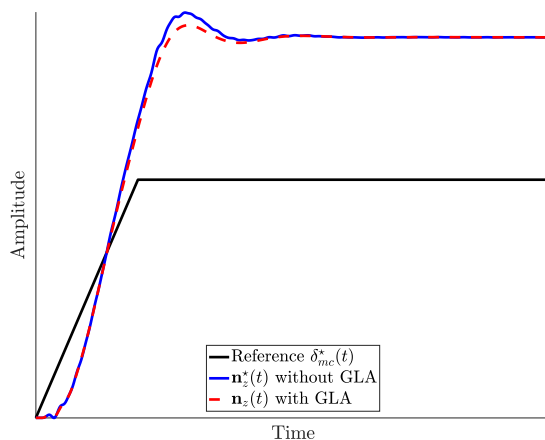


Figure 9: Time-domain response of the interconnection fig. 1 without (solid blue) and with (dashed red) the GLA function, to a pilot stick input (solid black).

In this paper, results are shown for few (worst case) configurations, but obviously, the entire process has been validated over all hundreds of cases and gust waves. This contributes in addressing both industrial safety and quality, as well as helping in the certification process. Moreover, all the presented tools were made available in the industrial process, running robustly in the workflow.

6.2 General contributions overview and improvements axes

The paper considers the challenge of GLA control function design and implementation while handling industrial constraints. Although this application is very challenging as it involves a family of complex medium-scale delayed models and considers different control specifications, both in time and frequency domains, authors believe that the process can be readily applied to any kind of complex linear dynamical systems.

Indeed, the main message of the article is to place *interpolatory methods* at the center of the modelling, design and discretisation steps. The main contributions of the paper can then be viewed from three angles. First, from a *methodological point of view*, the proposed process is flexible, numerically affordable and tailored to any (finite and infinite dimensional) linear dynamical models. Second, from a more *theoretical point of view*, it provides a complete view of interpolatory methods for dynamical systems, applicable to both realisation-based and transfer function-based models. Finally, algorithm 1 gives a complete process to perform a dynamical model/controller discretisation resulting in an alternate solution to the classical literature methods, standing then as a third, *algorithmic* contribution.

References

- [1] M. ALAMA, M. HROMCIKB, AND T. HANIS, *Active gust load alleviation system for flexible*

- aircraft: Mixed feedforward/feedback approach*, Aerospace Science and Technology, 41 (2015), pp. 122 – 133.
- [2] D. AMSALLEM AND C. FARHAT, *An online method for interpolating linear parametric reduced-order models*, SIAM Journal of Scientific Computing, 33 (2011), pp. 2169–2198.
- [3] A. ANTOULAS, *The Loewner framework and transfer functions of singular/rectangular systems*, Applied Mathematics Letters, 54 (2016), pp. 36–47.
- [4] A. ANTOULAS, C. BEATTIE, AND S. GUGERCIN, *Interpolatory methods for model reduction*, SIAM Computational Science and Engineering, Philadelphia, 2020.
- [5] A. ANTOULAS, S. LEFTERIU, AND A. IONITA, *Model reduction and approximation theory and algorithms*, SIAM, Philadelphia, P. Benner, A. Cohen, M. Ohlberger and K. Willcox Eds, 2016, ch. A tutorial introduction to the Loewner framework for model reduction.
- [6] A. C. ANTOULAS, I. V. GOSEA, AND A. C. IONITA, *Model reduction of bilinear systems in the Loewner framework*, SIAM Journal on Scientific Computing, 38 (2016), pp. B889–B916.
- [7] P. APKARIAN AND D. NOLL, *Nonsmooth \mathcal{H}_∞ Synthesis*, IEEE Transaction on Automatic Control, 51 (2006), pp. 71–86.
- [8] B. BAMIEH, J. BOYD PEARSON, B. FRANCIS, AND A. TANNENBAUM, *A lifting technique for linear periodic systems with applications to sampled-data control*, Systems & Control Letters, 17 (1991), pp. 79 – 88.
- [9] L. BARATCHART, *Existence and Generic Properties of L^2 Approximants for Linear Systems*, IMA Journal of Mathematical Control & Information, 3 (1986), pp. 89–101.
- [10] L. BARATCHART, M. CARDELLI, AND M. OLIVI, *Identification and rational \mathcal{L}_2 approximation: A gradient algorithm*, Automatica, 27 (1991), pp. 413–417.
- [11] A. BUNSE-GERSTNER, D. KUBALINSKA, G. VOSSEN, AND D. WILCZEK, *h_2 -norm optimal model reduction for large scale discrete dynamical MIMO systems*, Journal of Computational and Applied Mathematics, 233 (2010), pp. 1202–1216.
- [12] T. CHEN AND B. FRANCIS, *Input-output stability of sampled-data systems*, IEEE Transactions on Automatic Control, 36 (1991), pp. 50–58.
- [13] T. CHEN AND B. FRANCIS, *Optimal sampled-data control systems*, Springer Science & Business Media, 1995.
- [14] R. GADIANT, E. LAVRETSKY, AND K. WISE, *Very Flexible Aircraft Control Challenge Problem*, in Proceedings of the AIAA Guidance, Navigation, and Control Conference, Minneapolis, Minnesota, USA, August 2012.
- [15] K. A. GALLIVAN, A. VANDEROPE, AND P. VAN DOOREN, *Model reduction of MIMO systems via tangential interpolation*, SIAM Journal of Matrix Analysis and Application, 26 (2004), pp. 328–349.
- [16] K. GLOVER, *All Optimal Hankel Norm Approximation of Linear Multivariable Systems, and Their \mathcal{L}_∞ error Bounds*, International Journal Control, 39 (1984), pp. 1145–1193.
- [17] I. GOSEA AND A. ANTOULAS, *Stability preserving post-processing methods applied in the Loewner framework*, in Workshop on Signal and Power Integrity, 2016, pp. 1–4.
- [18] S. GUGERCIN, A. C. ANTOULAS, AND C. A. BEATTIE, *\mathcal{H}_2 Model Reduction for Large Scale Linear Dynamical Systems*, SIAM Journal on Matrix Analysis and Applications, 30 (2008), pp. 609–638.

- [19] N. HIGHAM, *Accuracy and stability of numerical algorithms (2nd edition)*, SIAM, 2002.
- [20] T. KIER AND G. LOOYE, *Unifying manoeuvre and gust loads analysis models*, in Proceedings of the International Forum on Aeroelasticity and Structural Dynamics, July 2009.
- [21] M. KOHLER, *On the closest stable descriptor system in the respective spaces \mathcal{RH}_2 and \mathcal{RH}_∞* , Linear Algebra and its Applications, 443 (2014), pp. 34–49.
- [22] R. B. LEHOUCQ AND D. C. SORENSSEN, *Deflation Techniques for an Implicitly Restarted Arnoldi Iteration*, SIAM Journal on Matrix Analysis & Applications, 17 (1996), pp. 789–821.
- [23] J. MARI, *Modifications of rational transfer matrices to achieve positive realness*, Signal Processing, 80 (2000), pp. 615–635.
- [24] A. J. MAYO AND A. C. ANTOULAS, *A framework for the solution of the generalized realization problem*, Linear Algebra and its Applications, 425 (2007), pp. 634–662.
- [25] C. MEYER, G. BROUX, J. PRODIGUE, O. CANTINAUD, AND C. POUSSOT-VASSAL, *Demonstration of innovative vibration control on a Falcon Business Jet*, in Proceedings of the International Forum on Aeroelasticity and Structural Dynamics, Como, Italy, June 2017.
- [26] D. OSSMANN AND C. POUSSOT-VASSAL, *Design and assessment of a two degree of freedom gust load alleviation system*, in Euro GNC, Milan, Italy, April 2019.
- [27] D. PETERSSON AND J. LOFBERG, *Model reduction using a frequency-limited \mathcal{H}_2 -cost*, System & Control Letters, 67 (2014), pp. 32 – 39.
- [28] I. PONTES DUFF, C. POUSSOT-VASSAL, AND C. SEREN, *Optimal \mathcal{H}_2 model approximation based on multiple input/output delays systems*, Systems & Control Letters, 117 (2018), pp. 60–67.
- [29] C. POUSSOT-VASSAL, *Large-scale dynamical model approximation and its applications*, HDR, habilitation thesis, Onera, INP Toulouse, Toulouse, France, July 2019.
- [30] M. PUSCH, *Allocation of Distributed Flaps for Gust Load Alleviation*, in Proceedings of the Conference on Control Technology and Application, Waimea, USA, July 2018, pp. 27.8–30.8.
- [31] M. PUSCH, D. OSSMANN, J. DILLINGER, T. KIER, M. TANG, AND J. LUBKER, *Aeroelastic modeling and control of an experimental flexible wing*, in Proceedings of the AIAA Scitech 2019 Forum, 2019, p. 0131.
- [32] D. QUERO, *An Aeroelastic Reduced Order Model for Dynamic Response Prediction to Gust Encounters*, PhD thesis, Technical University of Berlin, 2017.
- [33] D. QUERO, P. VUILLEMIN, AND C. POUSSOT-VASSAL, *A Generalized State-Space Aeroserovoelastic Model based on Tangential Interpolation*, Aerospace, (2019).
- [34] Y. SAAD, *Iterative Methods for Sparse Linear Systems*, SIAM, Philadelphia, 2000.
- [35] Y. SAAD AND M. SCHULTZ, *GMRES: A generalized minimal residual algorithm for solving nonsymmetric linear systems*, SIAM Journal of Scientific and Statistical Computing, 7 (1986), pp. 856–869.
- [36] G. SLEIJPEN AND H. VAN DER VORST, *A Jacobi-Davidson iteration method for linear eigenvalue problems*, SIAM Journal on Matrix Analysis and Applications, 17 (1996), pp. 401–425.
- [37] J. SPANOS, M. MILMAN, AND D. MINGORI, *A new algorithm for \mathcal{L}_2 optimal model reduction*, Automatica, 28 (1992), pp. 897–909.
- [38] P. VAN DOOREN, K. A. GALLIVAN, AND P. A. ABSIL, *\mathcal{H}_2 -optimal model reduction of MIMO systems*, Applied Mathematics Letters, 21 (2008), pp. 53–62.

- [39] P. VAN DOOREN, K. A. GALLIVAN, AND P. A. ABSIL, *\mathcal{H}_2 -optimal model reduction with higher order poles*, SIAM Journal on Matrix Analysis and Applications, 31 (2010), pp. 2738–2753.
- [40] C. D. VILLEMAGNE AND R. E. SKELTON, *Model Reduction using a Projection Formulation*, International Journal Control, 40 (1987), pp. 2141–2169.
- [41] P. VUILLEMIN, *Frequency-limited approximation of large-scale LTI dynamical models*, Ph.D. thesis, Onera, ISAE, Toulouse University, Toulouse, France, November 2014.
- [42] P. VUILLEMIN AND C. POUSSOT-VASSAL, *Discretisation of continuous-time linear dynamical model with the Loewner interpolation framework*, arXiv 1907.10956, (2019).
- [43] P. VUILLEMIN, C. POUSSOT-VASSAL, AND D. ALAZARD, *\mathcal{H}_2 optimal and frequency limited approximation methods for large-scale LTI dynamical systems*, in Proceedings of the 6th IFAC Symposium on Systems Structure and Control, Grenoble, France, February 2013, pp. 719–724.
- [44] P. VUILLEMIN, C. POUSSOT-VASSAL, AND D. ALAZARD, *Spectral expression for the Frequency-Limited \mathcal{H}_2 -norm of LTI Dynamical Systems with High Order Poles*, in Proceedings of the 13th European Control Conference, Strasbourg, France, June 2014, pp. 55–60.
- [45] K. WILLCOX, J. PERAIRE, AND J. WHITE, *An Arnoldi approach for generation of reduced-order models for turbomachinery*, Journal of Computers & Fluids, 31 (2002), pp. 369–389.